JAST, Vol. 7, No. 1, pp 51–57

JAST
Journal of Aerospace Science and Technology

Effects of Pitching Motion on Shock Behavior in a Body-Wrap Around Fin Configuration

H. Fazeli[1], M.R. Soltani[2] and A.R. Davari[3]

The unsteady aerodynamic behavior of TTCP model with various wrap around fin sets were investigated in a trisonic wind tunnel. The aerodynamic coefficient force measurement in this wind tunnel shows good agreement in comparison with that of the NASA Langley Research Center in static case. The model was sinusoidally oscillated at three different frequencies of 1, 3 and 8 Hz at M=2.0 and the effects of these frequencies on the shock angle were investigated and compared with the corresponding static case. Experimental data indicate that the static shock angle does not fall between the upstroke and down stroke dynamic shock angle at different frequencies which is different from experimental findings for flat fin configurations. This unsteady behavior could be added to the other anomalies frequently seen in the aerodynamic characteristics of the wrap around fin configurations. Also, the shock development mechanism over the nose and several fin sets was investigated and the shock-boundary layer interaction near the fin/body juncture which leads to shock likes λ was clearly observed in this investigation.

INTRODUCTION

The term "wrap-around fin" (WAF) usually refers to a projectile stabilizing or control surface, which has the same curvature as the missile body, and is wrapped around the projectile until deployment. The curved surfaces fold tightly around the missile body, taking up little tube volume, a precious commodity in such a small bundle. When the missile clears the launcher, the fins, usually four evenly spaced around the circumference, spring out and lock. WAF configurations have conventional longitudinal aerodynamic characteristics similar to those with planar fins of identical planform [1]. However, aerodynamic anomalies exist in the form of a roll moment at zero angle of attack, a roll reversal near Mach 1.0, and the presence of a side force/moment at a nonzero angle of attack [2]. The phenomenon that the sign of the roll moment changes as Mach number increases is known as roll reversal.

Extensive theoretical, numerical and experimental research has been done on WAF configurations over the years. Dahlke [3-4] documented wind tunnel tests in which parametric studies of WAF configurations were tested at different Mach number ranges. The roll moment dependence of WAF configurations with Mach number is of great concern to designers in order to avoid spin-yaw resonance. Range tests [5, 6] have also indicated that the magnitude of rolling moment decreases with Mach number and that a second rolling-momentum reversal may occur at high supersonic speeds ($M \approx 4.5 - 4.7$). Recently, Azimi *et.al.* [7] has reproduced the secondary roll reversal using computational methods for the first time.

Among all of the aforementioned investigations which have been concerned experimentally or numerically with the WAF configurations, very few have focused on the dynamical behavior of a missile configuration with WAFs in an oscillatory motion in the wind tunnel. Unsteady aerodynamic effects, in general, have a major impact on the maneuverability and controllability of missiles and aircraft. In an oscillatory motion, the element of time makes the flow pattern more complicated. During an oscillation in pitch, the

1. *(Corresponding Author), Assistant Professor, Malek Ashtar Univ. of Tech., Tehran, Iran, Email: fazeli@mut.ac.ir.*
2. *Professor, Dept. of Aerospace Eng., Sharif Univ. of Tech., Tehran, Iran.*
3. *Associate Professor, Dept. of Mech. and Aerospace Eng., Islamic Azad Univ., Science and Research Branch, Tehran, Iran.*

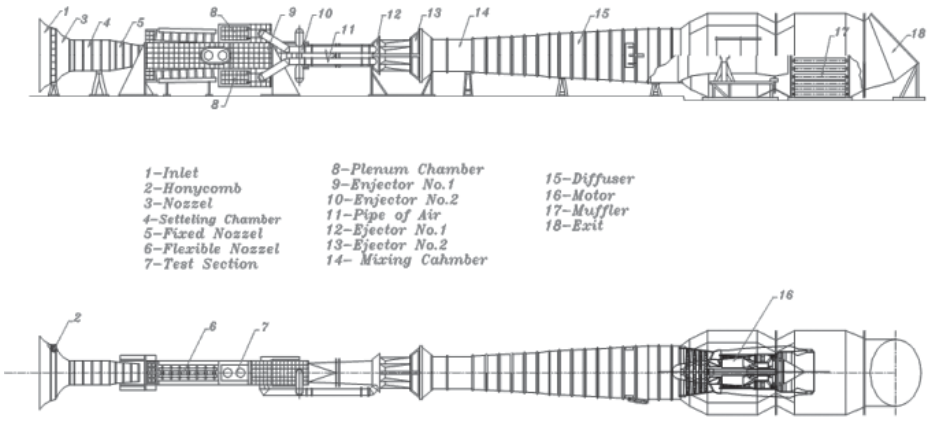

Figure 1. The schematic of view of QRC wind tunnel.

lateral and vertical position of vortices change as a function of the angle of attack, which itself is a function of time. Similarly, vortices periodically vary their longitudinal location at which they burst. The various components of an aircraft or a missile move in and out of the local flow regions in which they are embedded [8]. All of these motions do not take place in a manner simultaneous with the aircraft or missile motion, but with a certain delay mainly due to the convective time lag which is a function of the distance between the station under consideration and the station at which a particular flow phenomenon originates. This delay is mainly due to the fluid inertia and can be considered as the main source of the hysteresis loops observed in the force and moment variations with angle of attack for a vehicle in an oscillatory motion.

WIND TUNNEL AND MODEL

All tests were conducted in the trisonic wind tunnel of Qadr Research Center, QRC. This tunnel is of open-circuit blow down type and operates continuously between Mach numbers 0.4-4.2, via engine RPM and nozzle adjustments. It has a test section of $60 \times 60 \times 120$ cm^3 and is equipped with various internal strain gauge balances for force and moment measurements. Figure 1 shows a schematic view of QRC wind tunnel and its different parts when this study was conducted.

Figure 2 shows photographs of the confiurations used in this study. The model consists of an ogival nose, a cylindrical aft body along with various fin shapes. In these figures from left to right, three fin shapes

Figure 2. Photographs of model with different fin set in the test section of wind tunnel.

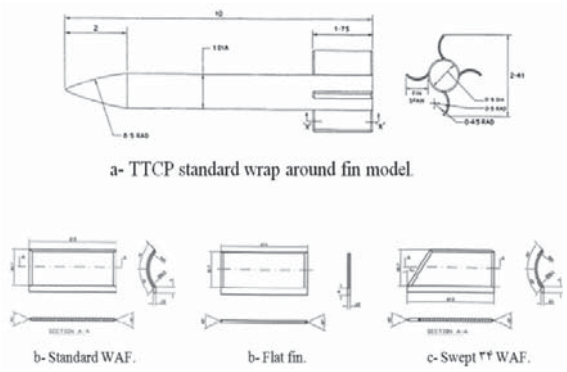

Figure 3. TTCP standard models and three different fin sets.

including flat plate, TTCP standard wraparound and 34 degrees swept wraparound ones are shown. The models shown in Figure 2 are located in the test section installed on an internal three or six component strain gauge balance.

Figure 3 shows The Technical Cooperation Program (TTCP) standard model along with three different fin sets used in this investigation.

In addition to force measurement, flow visualization was done in the wind tunnel using TTCP model with different fin sets through the schlieren system. Figure 4 shows the model installation mechanism in the wind tunnel along with the schlieren visualization system and its different parts used in QRC trisonic wind tunnel. The schlieren system is composed of two convex mirrors, a light source, a knife-edge plate and a digital camera for recording the pictures. Using this apparatus, one can observe the shock development mechanism in the test section or over the model instantaneously. Also, the detail of this development can be observed and studied using slow motion or frame by frame picture if desired.

In the coming section, the shock development mechanism over the nose and several fin sets used for

this detailed investigation will be shown and explained.

SHOCK DEVELOPMENT SYSTEM

As was previously indicated, the trisonic tunnel is of open type, driven by a jet engine located at the end of the tunnel; hence, it takes some time for the flow inside the test section to reach the desired Mach number. Figure 5 shows the shock development system on the nose of the model at zero angle of attack. The presence of expansion wave on the model shoulder is an indication of transonic speed. At this Mach number, the flow over the nose accelerates, reaching supersonic speed and expands at the junction between the nose and the body, Figure 5 (first three images of the first row from left to right). The flow speed increases as increasing the engine RPM; hence, the expansion waves become stronger.

This process is quite obvious from the images of the first row in Figure 5, until a normal shock stands in front of the nose of the model. At this particular speed, the flow behind the normal shock is subsonic,

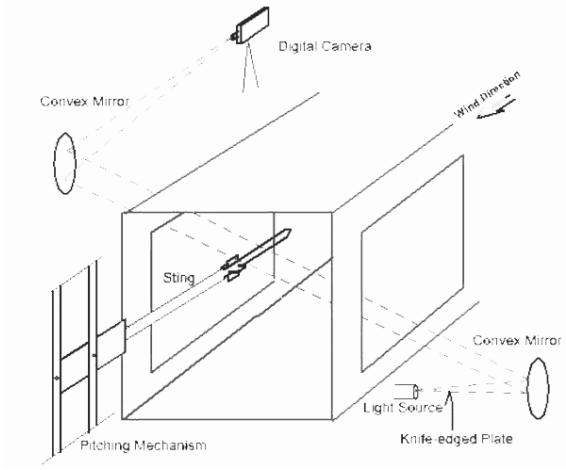

Figure 4. Schlieren camera and mirror set up.

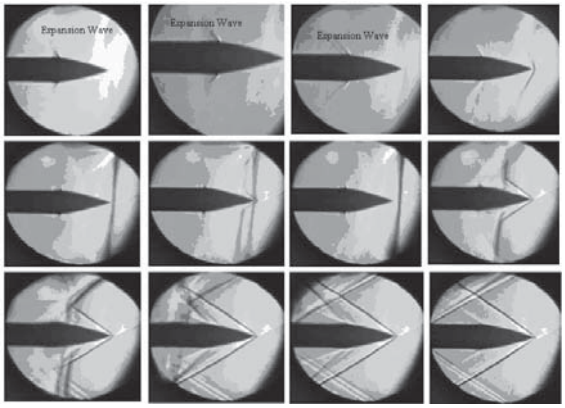

Figure 5. Schlieren images of shock development system over the nose of model.

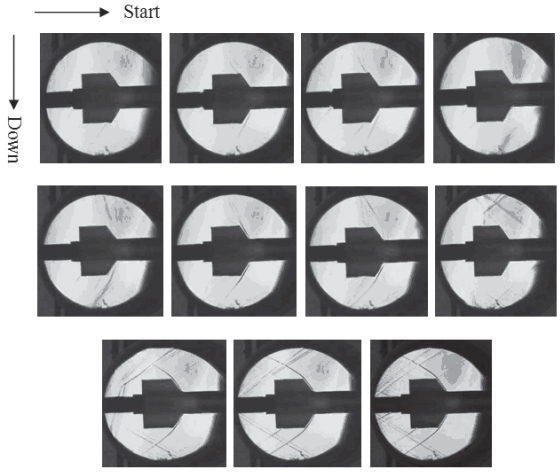

Figure 6. Schlieren images of the shock development system over the swept WAF.

but since the normal shock is not strong, $M \approx 1.0$, the flow speed behind it does not reduce drastically. The flow over the nose then accelerates, reaching supersonic speed and expands at the shoulder. As increasing the tunnel speed, this normal shock moves closer to the body, Figure 5, second row. Reaching to the nose of the model, the normal shock shows unsteady behavior and goes back and forward to the nose several times, and finally wraps itself around the body as it tries to pass the model, which is shown in the second row of Figure 5. From these images, formation of conical shocks or oblique shocks, as shown, is quite clear. Also, movement of the normal shock over the body and its interaction with the expansion waves at the shoulder can be clearly observed in the schlieren images, third row of Figure 5. As the normal shock passes the body, the flow behind it reaches its steady value of $M_\infty = 2.0$. At this stage the operator can start acquiring the force and moment data or pressure signature.

Figure 6 shows the same process explained for Figure 5, on the model fin systems. The fins shown in this figure are wraparound with a sweep angle of 34 degrees. Again, formation of expansion waves on the fin tips, passage of normal shock over the body and fins, and formation of oblique shocks at the beginning of the fins along with expansion waves at the end of the wraparound fins are clear in this figure. Also, formation of a jet liked flow at the tip of the fins is observed once the shock system has been established.

Figure 6 shows variations of the shock shape over the nose of the body with angle of attack at two degrees interval between 0.0 and 10.0 degrees and a Mach number of 2.0. For the zero angle of attack, the shock is symmetric as it should be, but as the angle of attack increases, the shock strength on the upper surface decreases, while the strength of the lower surface increases. The angle between the nose and the shock wave is an indication of the shock strength. As

seen in Figure 6, by increasing the angle of attack, the shock wave on the lower surface gets closer to the body, hence becoming stronger. Also shown in this figure, are the expansion waves formed at the junction of the nose and the body and their variations with the shock angle.

Figures 8-10 show the schlieren images of the variation of shock wave with the angle of attack formed over three different fins tested in these investigations. From these figures, one can clearly see the effects of fin shapes on the shock system formed over it. These variations affect the aerodynamic forces and moments developed by the model at various angles of attack.

In Figure 8, it is clearly visible that the shock-boundary layer interaction has produced a λ-shaped shock typically observed in front of blunt fins and cylinders mounted on flat plates in supersonic flowfields [29, 39]. It seems that the bow shock remains detached over the full height of the fins at zero angle of attack. At higher angles of attacks, the bow shock remains detached over the leeward fin at this Mach number. At one third of the upper section of the windward fin, the bow shock remains detached but attached over the reminder of this fin. In Figure 9, it seems that the bow shock over the WAFs remains attached at $M_\infty = 2.0$ and various angles of attack. The λ shock structure could be seen on the lower WAF near the fin/body juncture at zero angle of attack in this figure. This λ shock was observed to be unsteady, as its position was observed to shift slightly from photograph to photograph on standard WAFs at this Mach number and zero angle of attack. In Figure 10, it is clearly seen that the bow shock over the leading edge of the swept WAFs is detached at $M_\infty = 2.0$ and various angles of attack, although the structure at the fin/body intersection is somewhat obscured by the boundary layer on the model body. In Figures 8-10, two other oblique shocks are seen at the end of the fin sets near

Figure 7. Schlieren images of the nose at $M_\infty = 2.0$ and various angles of attack.

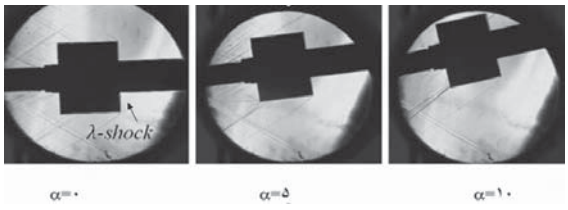

Figure 8. Schlieren images of the flat fin at $M_\infty = 2.0$ and various angles of attack.

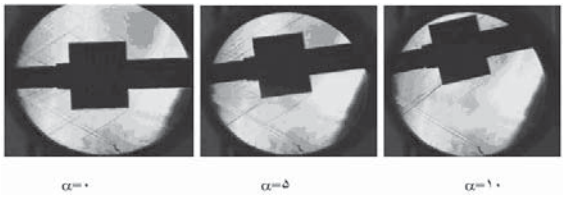

Figure 9. Schlieren images of the WAF at $M_\infty = 2.0$ and various angles of attack.

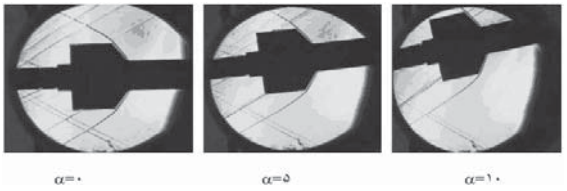

Figure 10. Schlieren image of the swept WAF at $M_\infty = 2.0$ and various angles of attack.

the attachment section of the sting and fin sets. These oblique shocks are caused by two steps on the sting. The other structures in the images which extend from the floor upward are 'seam shocks'. These disturbances are caused by small imperfections in the tunnel floor associated with removable plugs which are extended across most of the test section. Their strength is exaggerated in the photographs primarily due to their two-dimensional nature. In contrast, the bow and oblique shocks are three-dimensional structures.

Since the effects of fin shapes on the developed shock wave system can not be seen from Figures 8-10, the angle between the shock wave and the fin for three different fin sets at zero angle of attack are plotted in Figure 11 for $M_\infty = 2.0$. In this figure, it is seen that the shock wave for the flat fin is stronger than the wraparound and swept fin sets. Note that the shock strength depends on the angle between the shock and the body. The lower the angle, the stronger the shock wave; hence, a higher wave drag is obtained. Thus, it is expected that the flat fins cause higher wave drag than the other two sets when tested under similar conditions.

EFFECT OF OSCILLATION FREQUENCY ON THE SHOCK ANGLE

As indicated before, the models were sinusoidally oscillated at three different frequencies of 1, 3 and 8 Hz. The oscillation angle was 3 degrees and the model

Figure 11. Schlieren image of the fin sets at and $M_\infty = 2.0$.

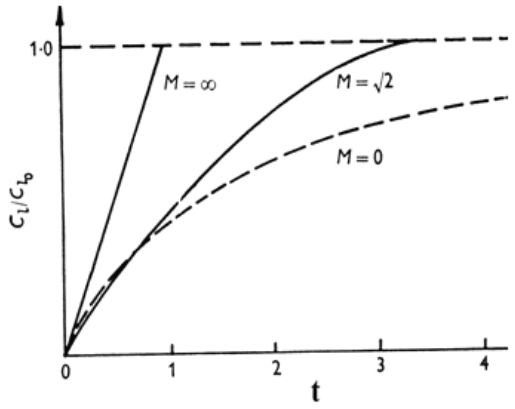

Figure 12. The growth of the lift on a two-dimensional airfoil vs. time, Ref. [9].

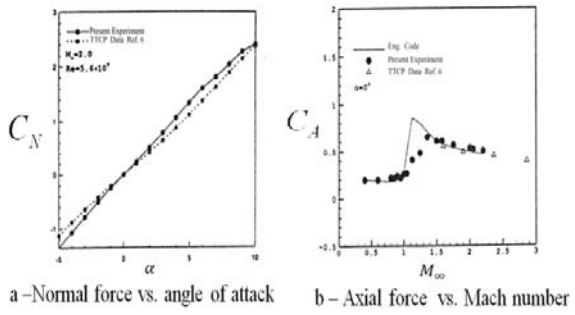

Figure 13. Comparison between the results of QRC and NASA wind tunnel.

was set at zero mean angle of attack. It has been reported that for subsonic case, aerodynamic loads vary differently with angle of attack during dynamic motions comparing to the static case. Substantial maximum force and moment overshoots, a delay in stall angle of attack and a large hysteresis between the increasing and decreasing angles of attack have been reported even for the very small oscillation frequency tested. This phenomenon is due to the lag in the flow-field over the

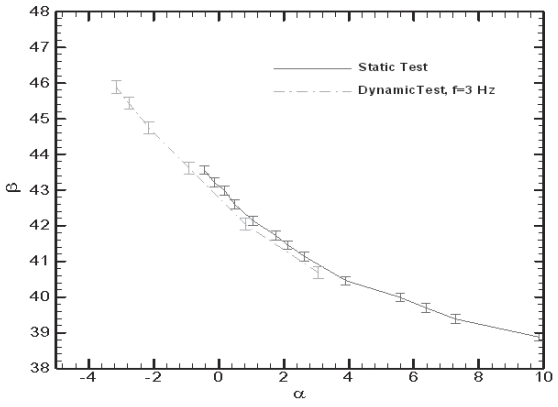

Figure 14. The uncertainty encountered in the static and dynamic shock angle measurements for a typical test.

model during the pitch up and pitch down motions. The flow patterns between the up-stroke and down-stroke motions are different for any particular angle of attack, creating the hysteresis loop. However, as the Mach number increases, the lag in the flow-field decreases and the time required for the aerodynamic forces and moments to reach their steady values also decreases. Figure 12 taken from reference [9] clearly shows this phenomenon. From this figure, note that at a very low speed, $M_\infty = 0.0$, it takes a long time for the dynamic lift coefficient to reach its static value; however, as the flow speed increases, $M_\infty = \sqrt{2}$ and beyond, the time required for the C_l to reach its steady value reduces dramatically. This figure clearly shows that for higher Mach numbers, the flow over the body adjusts itself to the variation of the angle of attack faster than that of the low number cases, hence one can conclude that for higher Mach numbers, especially in the supersonic case, variation of shock system formed over the body with time is similar to that of the static case for the similar angle of attack, at least for the low frequency ones.

In Figure 13, the aerodynamic coefficient force measurement between the QRC trisonic wind tunnel and that of the NASA Langley Research Center [10] is compared. Figure 13-a shows the normal force coefficient C_N vs. various angles of attack for TTCP standard model at $M_\infty = 2.0$ for two tunnels. Small differences between the results can be due to the precision in the manufacturing of the models. In Figure 13-b, the axial force coefficient C_A at zero angle of attack vs. Mach number is compared with the predicted results of Missile Datcom engineering code and the results of Ref. [10]. It is seen that there is good agreement between the experimental measurements.

The shock angle measurements were repeated for several oscillation cycles and the data have been then averaged over the upstroke and downstroke cycles individually. The average of the absolute deviations of the data points from their means for the static and dynamic cases were chosen as to be a characteristic for data uncertainty. Figure 14 shows the error bars indicating the uncertainties for both the static and dynamic data.

Figure 15 shows static and dynamic variations of the nose shock angle with the angle of attack for three different oscillation frequencies of 1, 3 and 8 Hz. at $M_\infty = 2.0$. For the dynamic case, the shock angle for both increasing (up-stroke) and decreasing (down-stroke) angles of attack, shown in these figures, are compared with their static values. As mentioned before, the shock angle, shown in Figure 15, corresponds to the lower shock formed at the nose of the body. From this figure, it is seen that for oscillation frequencies of 1 and 3 Hz., the shock angle variations with the angle of attack for both static and dynamic cases are

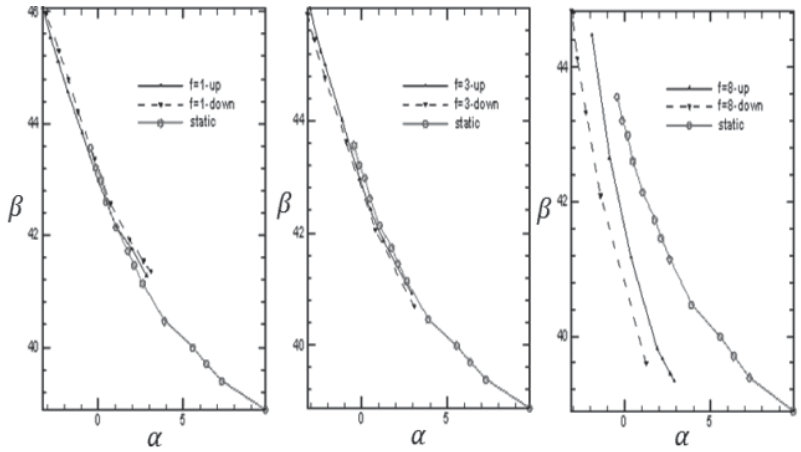

Figure 15. Dynamic and static nose shock angle variation vs. α for different oscillation frequencies.

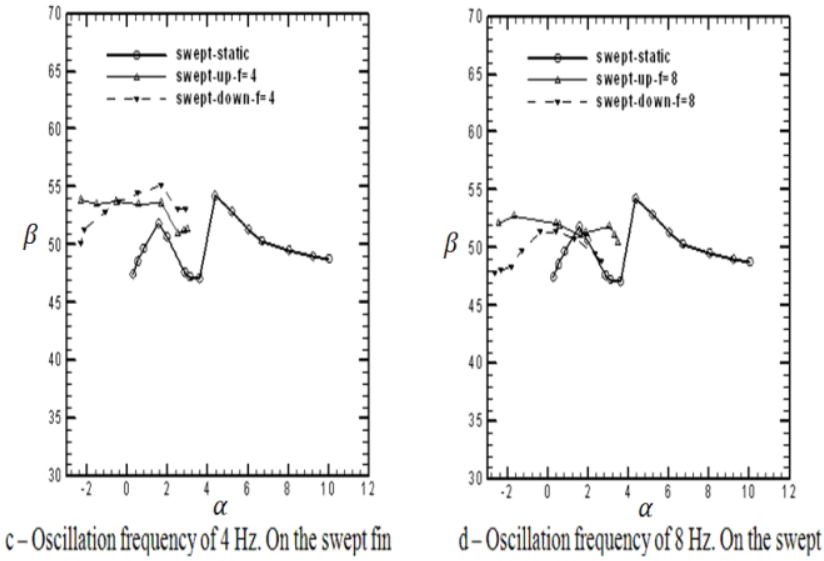

Figure 16. Variation of static and dynamic shock angles in front of the fin sets.

the same, Figures 15figures also illustrate that there is no hysteresis in the shock angle between the up-stroke and down-stroke motions. Hence, it could be concluded that for these oscillation frequencies, the shock system formed over the nose of the body does not lag or lead that of static cases. However, in Figure 15-b for the oscillation frequency of 3 Hz., a slight change in the shock angle could be seen, which varies with increasing and decreasing angle of attack.

Therefore; it is expected that for the higher oscillation frequencies, these variations and the hysteresis loop will be more pronounced. Figure 15-c shows dynamic variation of the shock angle with alpha for oscillation frequency of 8 Hz. for both increasing and decreasing angles of attack. This figure clearly shows the influence of oscillation frequency on the shock angle at each angle of attack when compared with the corresponding static value. Further, for each angle of attack shown in this figure, Figure 15-c, the shock angles for the up-stroke and down-stroke motions are not the same, forming a hysteresis loop in the acquired data.

Figure 16 shows variations of static and dynamic shock angles formed in front of the fin sets for $M_\infty = 2.0$. Static shock angles versus angle of attack in front of the fin for three different fin sets are plotted on the same figure, Figure 16-a, for comparison. Dynamic data in front of the swept fin set for different oscillation frequencies are shown in Figure 16-b, c and d. Again, note that the oscillation amplitude was \3 degrees

while the static data are taken from zero to ten degrees. The shock angle for the increasing angle of attack and pitch up motion for each alpha during the pitch down motion create a hysteresis loop, mentioned previously. Data for other two oscillation frequencies are available, but since no remarkable difference in the shock angle was observed, are not presented in this paper.

CONCLUSION

A qualitative study has been conducted on some body-wrap-around fin configurations to investigate the impact of pitching motion on the unsteady behavior of the shock waves emanating from the nose and the curved fins. The balance data show that the longitudinal behavior of the wrap around fin configurations is nearly the same as that of the flat fin, while a remarkable difference is observed in the lateral derivatives. According to the shock angle measurements, the shock angle variations with the instantaneous angle of attack increase as increasing the oscillation frequency. Moreover, the oblique conical shock at the nose tends to get closer to the body as the oscillation frequency decreases.

REFERENCES

1. Lucero E.F., "Subsonic Stability and Control Characteristics of Configurations Incorporating Wrap-Around Surfaces", *Journal of Spacecraft And Rockets*, **13**(12), PP 740-745(1976).
2. Winchenbach G.L., Buff R.S., Whyte R.H. and Hathaway W.H., "Subsonic and Transonic Aerodynamics of a Wraparound Fin Configuration", *Journal of Guidance, Control, and Dynamics*, **9**(6), PP 627-632(1986).
3. Dhalke C.W., "Experimental Investigation of Several Wraparuond Fins on Bodies of Revolution from Mach 0.3 to 1.3", *Data Report, US Army Missile Command, Redstone Arsenal, Report No. RD-TM-71-12.*, (1971).
4. Dhalke C.W., "The Aerodynamic Characteristics of Wrap-Around Fins at Mach Numbers of 0.3 to 3.0", *Technical Report, US Army Missile Command Redstone Arsenal, LL, Report No. RD-77-40*, (1976).
5. Abate G.L., Winchenbach G.L., "Analysis of Wrap-Around Fin and Alternative Deployable Fin Systems for Missiles", *AGARD Flight Vehicle Integration Conf.*, Ankara, Turkey, (1995).
6. Swenson M.N., Abate G.L. and Whyte R.H., "Aerodynamic Test and Analysis of Wrap-Around Fins at Supersonic Mach Numbers Utilizing Design of Expriments", *AIAA Paper 94-0200*, (1994).
7. Azimi A., Fazeli H. and Farhanieh B., "Investigation of Mach Number Effects on Roll Moment of Wrap-Around-Fin Configurations Using Thin-Layer Navier-Stokes Equations", *The 13th Annular Conference of the Computational Fluid Dynamics, Society of CFD*, Canada, (2005).
8. Orlik-Ruckeman K.J., "Aerodynamic Aspect of Aircraft Dynamics at High Angles of Attack", *Journal of Aircraft*, **20**(9), PP 737-751(1983).
9. Miles J.W., *The Potential Theory of Unsteady Supersonic Flow*, Cambridge University Press, (1959).
10. Fournier R.H., "Supersonic Aerodynamic Characteristics of a series of Wrap-Around Fin Missile Configurations", *NASA, TM X-3461*, (1977).